Coupled Electronic and Structural Relaxation Pathways in the Postexcitation Dynamics of Rydberg States of $BaAr_N$ Clusters

A. Masson,[1,*] M.-C. Heitz,[2] J.-M. Mestdagh,[1] M.-A. Gaveau,[1] L. Poisson,[1] and F. Spiegelman[2]
[1]Laboratoire Francis Perrin, CNRS-URA 2453, CEA IRAMIS, Laboratoire Interactions, Dynamique et Lasers, F-91191 Gif-sur-Yvette Cedex, France
[2]Laboratoire de Chimie et de Physique Quantiques/IRSAMC, CNRS and Université de Toulouse (UPS), Université Paul Sabatier, 118 route de Narbonne, F-31062 Toulouse Cedex, France
(Received 13 March 2014; revised manuscript received 18 July 2014; published 19 September 2014)

We investigate, theoretically, the joint relaxation of orbital and structure in postexcitation dynamics of Rydberg states of cluster $BaAr_N$ ($N = 250$). Mixed quantum-classical dynamics is used to account for the nonadiabatic transitions among more than 160 electronic states, represented via a diatomics-in-molecules Hamiltonian. The simulation illustrates the complex multistep relaxation processes and provides detailed insight in the mechanisms contributing to the final-time experimental photoelectron spectrum.

DOI: 10.1103/PhysRevLett.113.123005 PACS numbers: 31.70.Hq, 31.50.Gh, 33.60.+q, 36.40.-c

Introduction.—Energy relaxation in guest-host systems following guest excitation is an important topic frequently met in photophysics, photochemistry, photobiology, or condensed matter physics. The associated mechanisms are known to contribute to important processes such as photobiological damages, photosynthetic light harvesting [1] and photovoltaic devices [2], or degradation of quantum information due to coupling with the environment [3]. Theoretical approaches which face the full complexity of these phenomena are still missing owing to the large number of electronic and geometrical degrees of freedom which are at play. Modeling the energy relaxation which follows the electronic excitation of atoms or molecules at the surface of or within an inert host cluster is a very attractive step for stimulating the emergence of such very general treatments [4–10]. The finite size of the cluster allows us to change the complexity of the phenomena which are at play by varying, independently, electronic and nuclear degrees of freedom. Hence, the theoretical approaches can be evaluated at the proper level of complexity. Most of the literature concerns rather low excitations (usually valence) where the host-dopant interaction reduces, essentially, to a localized perturbation. The current challenge is to address potentially more intricate situations involving Rydberg initial excitations in which the size of the excited electronic orbital of the dopant becomes comparable with the cluster dimension. For example, recent experimental results have given evidence for the existence of stable Rydberg states of $NaHe_N$ nanodroplets with high quantum numbers, corresponding to a charged $NaHe_N^+$ nanodroplet and an orbiting Rydberg electron [11]. Another recent publication has reported a femtosecond pump-probe experiment where a single barium atom bound to an argon cluster ($Ar_{\approx 750}$) is suddenly excited into a superposition of electronic states with Rydberg character in the vicinity of the $6s9p\,^1P$ atomic state and probed by ionization [12]. This revealed a complex multistep dynamics involving numerous electronic states coupled via deformations along several hundred nuclear degrees of freedom, whose theoretical description is a challenge. The present Letter aims to demonstrate, theoretically, the interplay between the size of the excited orbital and the solvation of the dopant atom by a finite size system within a numerical modeling involving the full electronic and vibrational degrees of freedom of the system. We consider the $BaAr_{250}$ cluster excited by a 100 fs laser pulse with 266 nm central wavelength. These parameters correspond to recent experiments [12] which we use as guideline for the presented theoretical modeling. In the simulation, the electronic and nuclear dynamics of the highly excited cluster is described in its full dimensionality, including more than 160 coupled electronic states, as well as the probe step leading to the photoelectron spectrum at final time. The complexity of the system prevents from a full quantum simulation, and we use a mixed quantum-classical approach, with the usual partition of electrons and nuclei as quantum and classical particles, respectively. A variety of such methods exists [13–15], differing mainly by the nature of the electronic force acting on the nuclei. Typically, the latter is either obtained from an average over the electronic degrees of freedom (Ehrenfest or mean field [16]) or from single electronic states, with sudden hops between them, as in the widely used molecular dynamics with quantum transitions method [17]. In the present Letter, the use of a diatomics-in-molecules (DIM) approach allows for an efficient calculation of the Hamiltonian matrix and of its gradients. Nevertheless, due to the large number of excited states involved, the exhaustive sampling of the initial conditions and hopping statistics would still be a huge computational effort. Thus, we take advantage of an Ehrenfest-based method, enabling

propagation in a diabatic basis and avoiding frequent costly diagonalizations. However, Ehrenfest dynamics may face the problem of an inappropriate mean-field potential when the forces on several electronic states are very different. As a consequence, we choose an intermediate approach, reducing the electronic wave packet to a single adiabatic state at regular time intervals and propagating a mean-field trajectory in between [18].

Potential energy surfaces.—The DIM Hamiltonian was built from a valence-bond description of $BaAr_N$, restricted to singlets. A DIM basis for $BaAr_N$ in an energy range below 5 eV can be defined in terms of singly and doubly excited singlet configurations of Ba up to state $^1P(6s10p)$, all Ar atoms remaining in the ground state. The Hamiltonian matrix elements were expressed in terms of diatomic contributions. The Ba-Ar interactions were fitted from *ab initio* calculations of the diatomic, namely, two-electron full configuration interaction with extensive Gaussian basis sets, mapped into a diabatic representation. A similar DIM model for $BaAr_N^+$ based on $BaAr^+$ states was built to simulate the photoelectron spectrum. The Supplemental Material [19] provides details on the DIM approaches, on the parametrization of the potentials and on the transition dipole moments.

Non adiabatic dynamics.—The sampling of the initial conditions for the cluster is obtained by a classical dynamics at 35 K, corresponding to the temperature estimated in the experiment [12]. Assuming a Gaussian pump pulse of width τ_a and a central frequency ω_a, the initial excited electronic wave packet (within first-order perturbation theory) is given by its coefficients in the adiabatic basis

$$C_m^{(a)}(t=0) \propto -i\mathcal{D}^{0m} e^{[-(\tau_a^2/4)(E_m-E_0-\omega_a)^2]}, \qquad (1)$$

where $\mathcal{D}^{0m}$ is the dipole transition moment from the ground state to an excited adiabatic state m with energy E_m. It is assumed that during the ultrashort pump pulse, the system has not undergone a nonadiabatic transition. To simulate the postexcitation dynamics, we used the mean field with quenching (MFQ) method proposed by Janecek *et al.* [18] where the electronic wave packet is collapsed to a single adiabatic state at regular intervals (Δt_q). This adiabatic state is chosen stochastically according to the weights of the different states in the electronic wave packet. The mean-field propagation is then restarted, after adjustment of the nuclear momenta in the direction of the difference of mean-field forces before and after the collapse to ensure total energy conservation. If this adjustment is found to be impossible, the quenching is canceled and the mean-field propagation is simply resumed without modification until the next attempt. The dynamics was run using a fourth order Runge-Kutta algorithm with different time steps for the electrons (6×10^{-2} fs) and the nuclei (1.2 fs). In the MFQ method, the time interval $\Delta\tau_q$ between quenches is a parameter of the simulation. Test calculations on the smaller system $BaAr_{55}$ show the stability of the results within the range $\Delta\tau_q = 50$–100 fs. The parameters of the simulation are given in Table I.

TABLE I. Data for the simulation.

Initial temperature		35 K
Number of trajectories		300
Δt_q		50 fs
Trajectory duration		21.5 ps
Pump	ω_a	4.68 eV
	τ_a	100 fs
Probe	ω_b	3.12 eV
	τ_b	100 fs
DIM matrix size	$BaAr_N$	167
	$BaAr_N^+$	9

Results and discussion.—In the ground state, Ba is located at the surface of the Ar cluster. This determines the initial geometric conditions sampled for the excited state dynamics [see Fig. 1, where the chosen indicators are the distance between Ba and the closest Ar atom (left) and the distance of Ba to the center of mass of the argon cluster (right)]. Immediately after the pump pulse, the electronic wave packet is mainly developed on Rydberg states

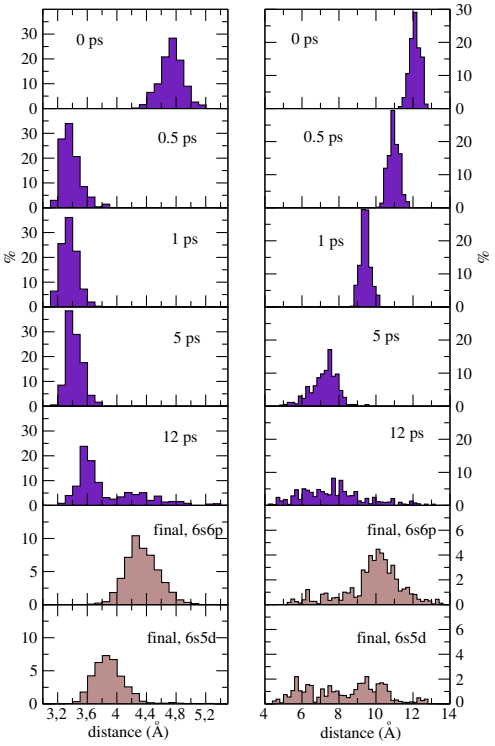

FIG. 1 (color online). Time evolutions of the Ba-to-closest-Ar distance (left) and of the Ba-to-center-of-mass of the Ar cluster distance (right) (evaporated Ar atoms are excluded when calculating the center of mass of the cluster). The data in the lowest panels are sorted according to the final channels and averaged between 20 and 21 ps.

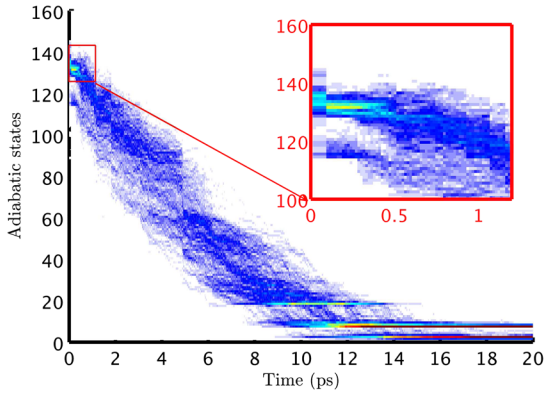

FIG. 2 (color online). Time evolution of the population of the adiabatic states labeled by their energy ordering number. Increasing populations from blue to red.

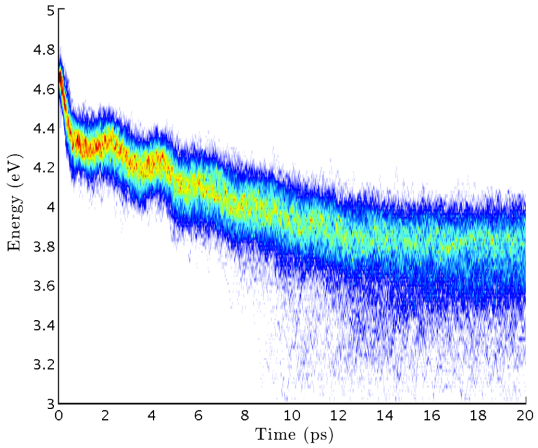

FIG. 3 (color online). Time evolution of the mean-field energies distribution.

($n \approx 9, 10$). The typical mean radius of the most contributing Rydberg orbitals is around 16 Å, and the corresponding electron cloud, thus, encloses, at least partially, the argon cluster whose diameter is about 25 Å. As a consequence, a large number of argon atoms are subjected to a polarization force due to the Ba^+ ion, only weakly screened by the diffuse Rydberg electron. Thus, during the first 0.5 ps, the argon density around Ba increases and Ba starts to move inside the cluster (see Fig. 1). Figure 1 of the Supplemental Material [19] shows the distribution of the number of Ar in a sphere of radius 4 Å surrounding the Ba atom at 500 fs. This rapid nuclear relaxation is basically an adiabatic process, as can be seen in Fig. 2 (inset): the population of the adiabatic states remains approximately constant during the first 350 fs. Although the adiabatic states population does not vary strongly during this step, the mean electronic energy drops from 4.68 eV (energy of the pump) to about 4.3 eV (Fig. 3). This is due to the stabilization of the core of the Rydberg state by the rearrangement of the argon environment. This relaxation step is consistent with previous studies about the stability of $NaAr_N^*$ excited states [20]. A second mechanism turns on between 0.5 an 10 ps. After the initial nuclear relaxation has converted electronic energy into kinetic energy, hence, heating the cluster, vibrational excitations induce nonadiabatic transitions. This can be seen in Fig. 2 where the populations of the adiabatic states shift to the lower states (from $m = 130$–134 initially to around $m = 20$ at 10 ps). This electronic relaxation leads to a decay of the electronic energy down to 3.8 eV (Fig. 3). During this time, the Ba atom continues to enter the argon cluster (Fig. 1, right). At longer times (starting from 12 ps up to 20 ps), intracluster electronic relaxation ends up populating essentially valence excited state manifolds like $6s6p$ or $6s5d$, followed by structural relaxation (Fig. 1) and evaporation of a small number of Ar atoms (at most 15) from the cluster. The most frequent final situation consists of Ba atoms in the $6s6p$ configurations which have drifted to the surface of the cluster (Fig. 1, second to last panels). The second channel corresponds to relaxation in the final $6s5d$ atomic valence states, with a more compact argon environment around the hosted atom (Fig. 1, lowest panels). At $t = 20$ ps, considered to be the final distribution, the Ba atoms in the $6s6p$ state have drifted to the surface of the cluster, while the ones in the $6s5d$ manifold are distributed between volume and surface solvation as indicated by the broad distribution shown in Fig. 1 (right panel). A further indication of this situation is given in the Supplemental Material [19], where the solvation of the Ba atoms at 20 ps is analyzed. The difference in the final solvation situation for the two electronic channels can be rationalized considering simple electronic considerations. The BaAr diatomic potentials correlating with $6s5d$ atomic states are globally more attractive than those correlating with the $6s6p$ manifold, with dissociation energies of 159, 73, and 60 cm^{-1} versus 114 and 43 cm^{-1}. Even if the potential energies are not additive, these quantities, compared to the ArAr binding energy of 99 cm^{-1}, rationalize the trend for a Ba atom in a $6s5d$ state to remain, at least for a longer time, inside the cluster. The relative values of the dissociation energies are connected to the respective radii of the excited orbital, which are 2.0 vs 3.5 Å for a $5d$ and a $6p$ orbital of Ba, respectively. This rationalizes the difference of the solvation in terms of a simple picture based on the size of the excited orbital. To make contact with recent experimental results, we have simulated the photoelectron spectra (PES) obtained from ionization with an ultrashort probe pulse interacting at a long delay time T after the pump pulse. Considering a Gaussian laser pulse of central frequency ω_b (Table 1) and assuming a direct ionization from any electronic state m to any ionic electronic states m', the electron signal can be approximated as [9]

$$P(E,T) = \sum_{\text{traj},m,m'} \mathcal{D}^{mm'2} |C_m^{(a)}(T)|^2 e^{[-(\omega_{mm'}+E-\omega_b)^2(\tau_b^2/2)]}, \quad (2)$$

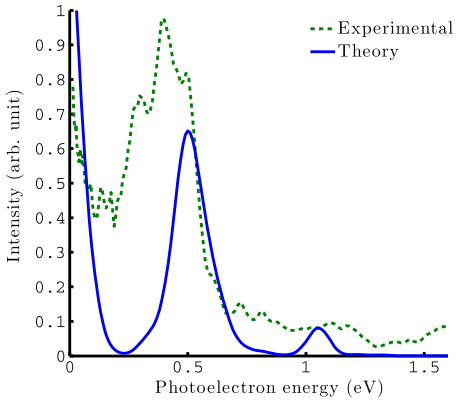

FIG. 4 (color online). Long time photoelectron spectra averaged in the interval 18–20 ps [green: experiment [12], blue: theory (arbitrary units)].

where "traj" labels a given trajectory, $\mathcal{D}^{mm'}$ are the neutral to ionized states transition dipole moments, E is the ejected electron energy and $\omega_{mm'} = E^i_{m'} - E_m$ are the ionization potentials. Full comparison between experimental [12] and theoretical PES as a function of the pump-probe delay is beyond the scope of the present Letter. Figure 4 shows a comparison at long delay time, and we note the good agreement between experiment and theory. Thus, we can interpret and assign the observed bands: the photoelectron band at 0.5 eV originates mainly from the $6s6p$ surface final channel, while the low energy band around 0.1 eV corresponds to the $6s5d$ states. Some minor contributions, including the additional band at 1.1 eV, stem from other existing embedded excited singlet channels, with significant components on Rydberg states of Ba initially higher than $6s10s$ but strongly stabilized in the compact environment. The experimental signal [12] is attributed to both solvated and free barium (singlet and triplet). No ejection of atomic barium appears in the present work where only singlet state dynamics is considered. Simulation of the ionization from triplet atomic states, as observed in the experiment would imply inclusion of spin-orbit coupling in the dynamics. But it is worthwhile to note that the calculated PES is in good agreement with the experimentally attributed signal coming from solvated Ba [12].

Conclusion.—The present Letter highlights the feasibility of a simulation of the nonadiabatic behavior of a large system via the MFQ method including both electronic and nuclear complexities. It demonstrates the strong interplay between the nature or level of the electronic excitation of a chromophore and its solvation by a rare-gas cluster. In consistency with what was inferred from the experiment [12], a clear physical picture of the relaxation process was unraveled by the present calculation. First, Rydberg excitation of Ba leads to its embedding inside the cluster, as an energetically favorable $BaAr_N^+$ core, with a diffuse electron. Subsequently, the coupling of electronic and vibrational motion induces a cascade of nonadiabatic transitions to the valence states, followed principally by the backmigration of Ba towards the surface of the cluster. The identification of two final distinct competitive electronic channels, which were not clearly anticipated in the experimental work, sheds light on the recorded long-time photoelectron spectrum. The details of solvation dynamics of these final states are seen to be related to the difference in size of the excited orbitals. The overall relaxation dynamics is an original illustration of finite size effects induced by the evolution of the relative extension of the excited electron versus the cluster solvent.

The authors acknowledge support from CNRS (Grant No. GDR 3533), Triangle de la Physique (Grant No. NOSTADYNE 2010-004-T), and the Toulouse computer facility CALMIP. We thank F. X. Gadea for helpful discussions and A. Scemama for technical help.

*Present address: Laboratoire de Chimie Physique Moléculaire, Ecole Polytechnique Fédérale de Lausanne, 1015 Lausanne, Switzerland

[1] Y. C. Cheng and G. R. Fleming, Annu. Rev. Phys. Chem. **60**, 241 (2009).
[2] G. D. Scholes, G. R. Fleming, A. Olaya-Castro, and R. van Grondelle, Nat. Chem. **3**, 763 (2011).
[3] G. A. Alvarez and D. Suter, Phys. Rev. Lett. **107**, 230501 (2011).
[4] C. P. Schulz, P. Claas, and F. Stienkemeier, Phys. Rev. Lett. **87**, 153401 (2001).
[5] B. Grüner, M. Schlesinger, Ph. Heister, W. T. Strunz, F. Stienkemeier, and M. Mudrich, Phys. Chem. Chem. Phys. **13**, 6816 (2011).
[6] A. I. Krylov, R. B. Gerber, M. A. Gaveau, J. M. Mestdagh, B. Schilling, and J. P. Visticot, J. Chem. Phys. **104**, 3651 (1996).
[7] R. Baumfalk, N. H. Nahler, U. Buck, M. Y. Niv, and R. B. Gerber, J. Chem. Phys. **113**, 329 (2000).
[8] M. Briant, M. A. Gaveau, J. M. Mestdagh, and J. P. Visticot, J. Chem. Phys. **112**, 1744 (2000).
[9] M.-C. Heitz, L. Teixidor, N.-T. Van-Oanh, and F. Spiegelman, J. Phys. Chem. A **114**, 3287 (2010).
[10] D. Zanuttini, J. Douady, E. Jacquet, E. Giglio, and B. Gervais, J. Chem. Phys. **134**, 044308 (2011).
[11] E. Loginov and M. Drabbels, Phys. Rev. Lett. **106**, 083401 (2011).
[12] A. Masson, L. Poisson, M.-A. Gaveau, B. Soep, J.-M. Mestdagh, V. Mazet, and F. Spiegelman, J. Chem. Phys. **133**, 054307 (2010).
[13] J. C. Tully, Faraday Discuss. **110**, 407 (1998).
[14] N. L. Doltsinis, in *From Theory to Algorithms, Lecture Notes*, edited by J. Grotendorst, D. Marx, and A. Muramatsu, NIC Series Vol. 10 (John von Neumann Institute for Computing, Jülich, 2002), pp. 377–397.

[15] M. J. Bedard-Hearn, R. E. Larsen, and B. J. Schwartz, J. Chem. Phys. **123**, 234106 (2005).
[16] P. Ehrenfest, Z. Phys. **45**, 455 (1927).
[17] J. C. Tully, J. Chem. Phys. **93**, 1061 (1990).
[18] I. Janecek, S. Cintavá, D. Hrivňák, R. Kalus, M. Fárník, and F. X. Gadea, J. Chem. Phys. **131**, 114306 (2009).
[19] See Supplemental Material at http://link.aps.org/supplemental/10.1103/PhysRevLett.113.123005 for details of the DIM modeling and complementary data analysis.
[20] M. Ben El Hadj Rhouma, Z. Ben Lakhdar, H. Berriche, and F. Spiegelman, J. Chem. Phys. **125**, 084315 (2006).